Supporting Information

Senning et al. 10.1073/pnas.0908338107

SI Text

Materials and Methods. ***Yeast Strains and fluorescent labeling of mitochondria.*** To eliminate the polarized movements accompanying cell division, we exposed *S. cerevisiae* of mating type "a" to the alpha factor pheromone of the opposite mating type, which induces cells from the G1 stage of the cell cycle to the mating phase. We examined healthy cells (MYY290), cells treated with cytoskeletal inhibitors, and strains with mutations and deletions in known cytoskeletal proteins. In our first set of experiments, we targeted microfilaments (MFs) and microtubules (MTs) using Latrunculin-A and Nocodazole, respectively. We next studied mitochondrial dynamics in the yeast mutants act1-v159n and Arc18pΔ, which we selected for their involvement in actin polymerization. In Fig. S1, we show fluorescence micrographs of typical specimens.

In Table S1, we list the strains of *S. cerevisiae* that we used in this study. We selected MATa strains for their sensitivity to alpha factor, which shifts these cells into the mating phase of the cell cycle. To visualize mitochondria, we transformed the cells with pRS316, containing DsRed.T1 fused to the COX4 leader sequence. We cultured cells to log phase in SD media, before treating them with 100 μM alpha factor for 2 h. For our microtubule depletion experiments, we treated samples with Nocodazole at 30 μg/mL, followed by incubation for an additional 30–40 min. For our microfilament depletion measurements, we treated samples with Latrunculin-A at 200 μM for a 10-min incubation period.

In preparing our samples, we mounted them onto a thin 3% agarose pad using SD media and 10 μM alpha factor. We sealed the samples using valap to fuse the edges of a coverslip to the glass slide. To visualize MTs or actin microfilments, we performed antibody staining with rat anti-α-tubulin (YOL 1/2 from clontech) or Alexa-phalloidin-542, following a 3.7% paraformaldehyde fixative treatment (1). We conducted our studies of the effects of cytoskeletal inhibiting drugs on mitochondrial motility at 22 °C, the mutant act1-V159N (DDY 1493) and its parent (DDY1495) at 36 °C, and the mutant Arc18Δ and its wild-type parent BY4741 at 22 °C.

Fourier imaging correlation spectroscopy (FICS). We used the FICS technique to quantify the motions of yeast mitochondria in our studies. FICS is a phase-sensitive method to measure the displacements of fluorescently labeled objects as a function of spatial length scale and over a broad distribution of time scales. The approach is an efficient and highly sensitive means to perform uninterrupted data acquisition over extended periods, while minimizing the deleterious effects of sample photodegradation, instrument drift, and laboratory noise (2–4). The samples were placed at the focal plane of a fluorescence microscope where an excitation grating was generated by intersecting two vertically polarized laser beams (Fig. S2*A*). The fluorescence signal results from the spatial overlap of the grating with the positions of labeled mitochondrial segments (see Figs. S2*B* and *C*). The beam waist at the sample (≈40 μm) is wide enough to encompass ≈15–30 yeast cells, and the fringe spacing d_G is adjustable between 0.5 –1.2 μm. The wave vector $\mathbf{k} = (2\pi/d_G)\hat{\mathbf{i}}$ specifies the spatial length scale and orientation of the grating, where $\hat{\mathbf{i}}$ is a unit vector pointing in the direction of the x axis. Time-dependent positional fluctuations of mitochondria are described by $\delta n(\mathbf{r},t) = \sum_{i=1}^{N} A_i \delta[\mathbf{r} - \mathbf{r}_i(t)] - N\bar{A}/V$, where $\mathbf{r}_i$ is the center-of-mass position of the ith segment, A_i is its fluorescence intensity, V is the sample volume, and $\bar{A}$ is the average segment intensity.

The phase of the grating ϕ was modulated at the frequency 50 kHz, so that the fringes were swept at a much greater speed than an average filament can move. Using phase-synchronous detection of the modulated fluorescence, we determined the complex signal $\hat{N}_{\mathbf{k}}(t) = N^{-1/2} \sum_{i=1}^{N} A_i \exp i[\mathbf{k} \cdot \mathbf{r}_i(t)]$. The signal is the Fourier transform of the sampled mitochondrial distribution, defined at the wave vector of the excitation grating. As the mitochondrial filament positions fluctuate, the resultant signal monitored by our experiment evolves in time. In a typical experiment, we collect ≈524,000 data points at an acquisition frequency of 256 Hz, over a period of about 35 min. To quantify the time dependence of $\hat{N}_{\mathbf{k}}(t)$, we calculate the two-point time correlation function (TCF) $F(k,\tau) = \langle \hat{N}^*_{\mathbf{k}}(0)\hat{N}_{\mathbf{k}}(\tau)\rangle = \lim_{T\to\infty} \frac{1}{T}\int_0^T \hat{N}^*_{\mathbf{k}}(t')\hat{N}_{\mathbf{k}}(\tau + t')dt'$, where the angle brackets indicate the time integral, and τ is the interval separating successive measurements. We repeated our measurements 10–15 times, and after comparing them for consistency, we averaged them together. Error bars were calculated from the dispersion in the data. The TCF decays on a time scale associated with the movement of filaments across distances characteristic of the optical fringe spacing d_G. For a dilute system of noninteracting Brownian particles, the TCF is expected to decay as a single exponential $\exp(-\tau/\tau_0)$, with $\tau_0 = (k^2 D_0)^{-1}$ the average time required for a particle to diffuse the distance d_G with diffusion constant D_0. We expect deviations from diffusive behavior to reflect the nonrandom interactions of mitochondrial segments with cytoskeletal elements, in addition to the influence of other intracellular species. To account for these deviations, we adopt the general form for the TCF: $F_0 \exp\{-\frac{1}{6}k^2\langle \Delta r^2(\tau)\rangle\}$, where the mean-square-displacement $\langle \Delta r^2(\tau)\rangle = 6D\tau^{\alpha}$, D is a generalized diffusion coefficient, and α is a temporal scaling exponent.

Video microscopy and digital image analysis. We performed time-lapsed video measurements on our samples using a Nikon TE2000U fluorescence microscope with a 100×, numerical aperture 1.4, oil immersion objective lens (Nikon, Plan Apo). The excitation source was a continuous wave laser (Coherent, Compass 215M) at $\lambda_{ex} = 532$ nm, with power typically set below ≈1 mW. The epifluorescence was imaged using a CCD digital video camera (Hamamatsu Photonics Japan, ORCA-12AG) mounted to a side port of the microscope. The temperature of the sample was maintained using a Peltier thermoelectric stage and controller (20/20 Technology, BC-100). The Hamamatsu frame grabber supplied with the CCD (Hamamatsu Photonics Germany, Wasabi) was used to digitize sequences of $1,344 \times 1,044$ square pixel frames. The calibrated pixel dimension was $1\,\text{pixel} = 0.0685$ μm. A typical run consisted of 100 frames in sequence. The images were processed, and the mitochondria positions were tracked using automated numerical procedures described by Margineantu et al. (5).

1. Pringle JR, Adams AE, Drubin DG, Haarer BK (1991) Immunofluorescence methods for yeast. *Methods Enzymol* 194:565–602.
2. Knowles MK, Guenza MG, Capaldi RA, Marcus AH (2002) Cytoskeletal-assisted dynamics of the mitochondrial reticulum in living cells. *Proc Natl Acad Sci USA* 99:14772–14777.
3. Senning EN, Marcus, AH (2008) Fourier imaging correlation spectroscopy for studies of intracellular structure-function. *Meths Cell Biol* 90–117–137.
4. Knowles MK, Grassman TJ, Marcus AH (2000) Measurement of the dynamic structure function of fluorescently labeled complex fluids by Fourier imaging correlation spectroscopy. *Phys Rev Lett* 85:2837–2840.
5. Margineantu D, Capaldi RA, Marcus AH (2000) Dynamics of the mitochondrial reticulum in live cells using Fourier imaging correlation spectroscopy and digital video microscopy. *Biophys J* 79:1833–1849.

6. Smith BJ, Yaffe MB (1991) A mutation in the yeast heat-shock factor gene cause temperature-sensitive defects in both mitchondrial protein import and the cell cycle. *Mol Cell Biol* 11:2647–2655.

7. Belmont LD, Drubin DG (1998) The yeast V159N actin mutant reveals roles for actin dynamics in vivo. *J Cell Biol* 142:1289–1299

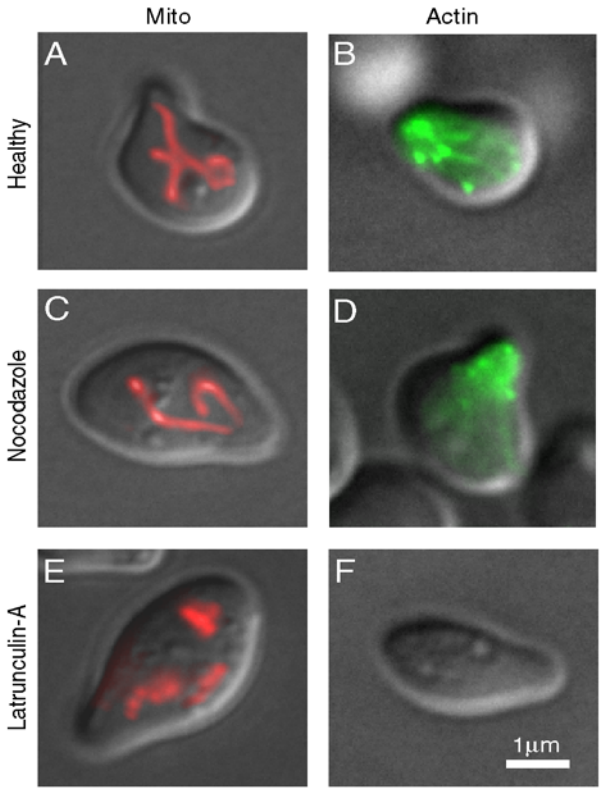

Fig. S1. Micrographs of fluorescently labeled yeast mitochondria (*Left*, red) and MFs (*Right*, green), under different (drug-induced) cytoskeletal conditions. For all the cases we studied, we observe the "shmoo" protrusion, characteristic of cells arrested in the mating state. For healthy yeast cells, mitochondrial structure is similar to that in higher organisms arrested in G1: a single interconnected network of tubular filaments constituting the reticulum morphology (2, 5) (*A*). (*B*), (*D*), and (*F*) show the results of alexa532-phalloidin labeling of actin filaments in fixed cells (see *SI Materials and Methods*). (*B*) shows that the actin cytoskeleton in healthy cells is extensive. Although prominent features such as actin cables and patches are concentrated near the shmoo tip, it is possible to discern diffuse actin filaments throughout the cytoplasm. For cells treated with the MT-destabilizing agent Nocodazole, both mitochondrial morphology (*C*) and actin filament integrity (*D*) appear to be unaffected. In contrast, the actin cytoskeleton of cells treated with Latrunculin-A appears depleted. In this case, the mitochondrial reticulum morphology is also disrupted, resulting in a population of intermediate size mitochondrial compartments (*E*). Our phalloidin labeling procedure reveals no trace of F-actin in Latrunculin-A treated cells (*F*).

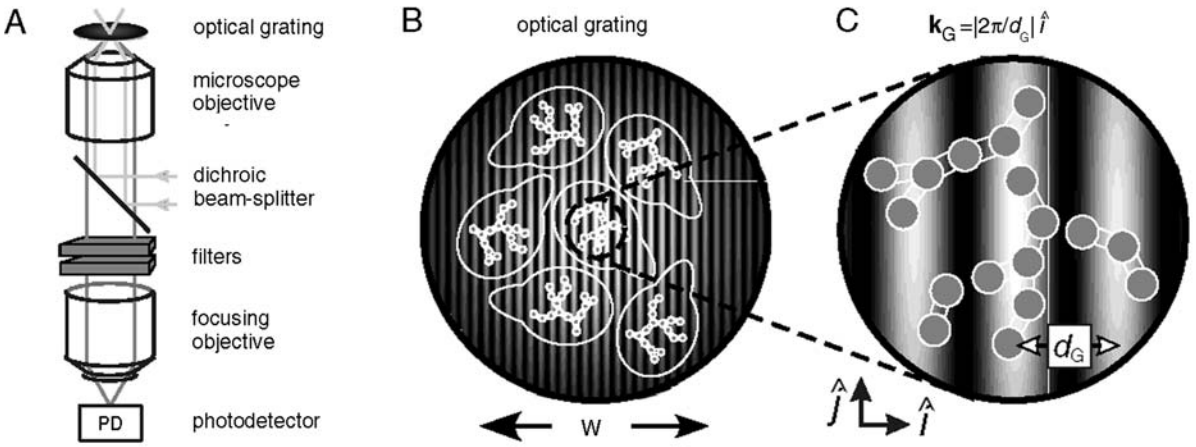

Fig. S2. Schematic diagram of the experimental geometry for FICS experiments, performed on fluorescently labeled yeast mitochondria (described in text).

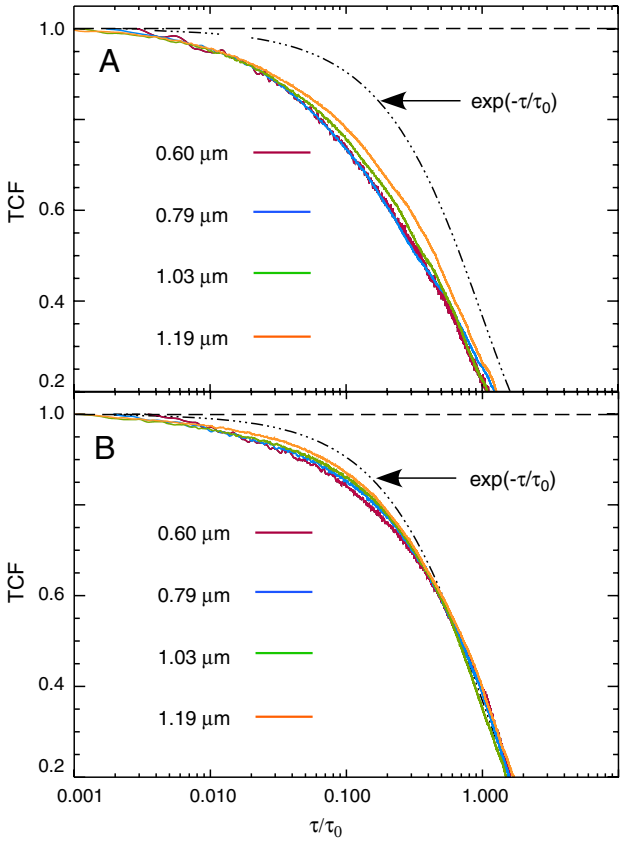

Fig. S3. Time correlation functions shown in Fig. 3 as a function of the reduced time variable τ/τ_0, with $\tau_0 = (k^2 D_0)^{-1}$ and $D_0 = 1.8 \times 10^{-4}$ $\mu m^2\, s^{-1}$. By plotting our data in this way, we rescale the TCFs to eliminate the contribution of random diffusion to the length scale dependence of the decays. For a system of independent Brownian particles, the TCFs measured at different length scales would all fall upon a single universal curve of the form $\exp(-\tau/\tau_0)$. We thus examine the length-scale-dependent influence of cytoskeletal proteins on mitochondrial mobility. In (*A*) we plot the TCFs for healthy cells, and in (*B*) we plot those for cells depleted of MFs. From the results shown in (*A*), we see that the TCFs do not lie on a single universal curve, indicating that mitochondria in healthy cells exhibit a length-scale-dependent, anomalous mobility beyond the effects of simple diffusion. The TCF corresponding to $d_G = 1.19$ μm appears to decay more slowly than for those with $d_G = 0.60$ μm and $d_G = 0.79$ μm, suggesting a trend of diminishing mobility with increasing distances. For cells depleted of MFs (*B*), the length-scale-dependence of the TCFs does not vanish. Instead, the regime of anomalous diffusion behavior appears to shift to shorter time scales. In both panels, we compare measured decays to the model single exponential function corresponding to random diffusion, with the time constant τ_0, which approximates the long-time (d_G-independent) relaxation of the data shown in (*B*). We compare the model decay to our data for healthy cells, shown in (*A*). We note that the value we have used for D_0 is the same as we obtained previously in experiments conducted on G1 arrested osteosarcoma cells, treated with microfilament and microtubule destabilizing agents (2). This suggests that the environment experienced by mitochondria in the absence of MTs and MFs is similar for yeast as for osteosarcoma cells.

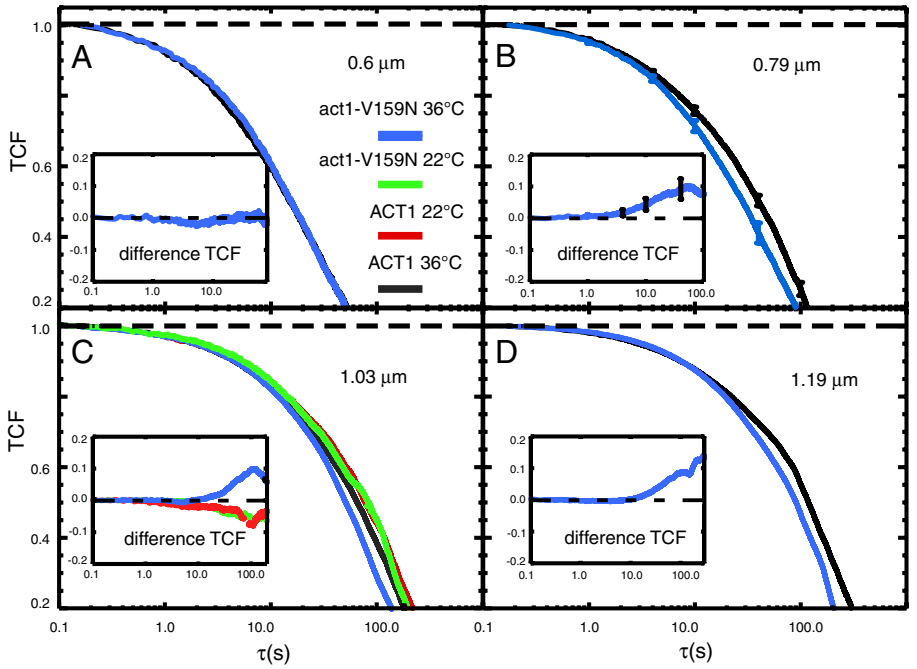

Fig. S4. Time correlation functions for act1-V159N studies. We compare TCFs from the actin mutant strain act1-V159N to those of its wild-type parent, which we measured at the elevated temperature of 36 °C. Each panel represents a different value for the probed length scale d_G. The act1-V159N strain is a temperature-sensitive mutation, whose cell culture growth rate is suppressed at the elevated temperature of 36 °C. At room temperature (22 °C), the growth rate of the mutant strain appears normal and is indistinguishable from its wild-type parent. At the elevated temperature, the decays of the TCFs for act1-V159N are faster than wild-type mitochondria for $d_G \geq 0.79$ μm [(*B–D*), and note error bars presented in (*B*)]. We find that this enhanced mobility vanishes when we decrease the sample temperature to 22 °C. This is shown for the length scale $d_G = 1.03$ μm (*C*), where we compare the TCFs of the room temperature wild-type parent (red curve) to the mutant act1-V159N (green curve).

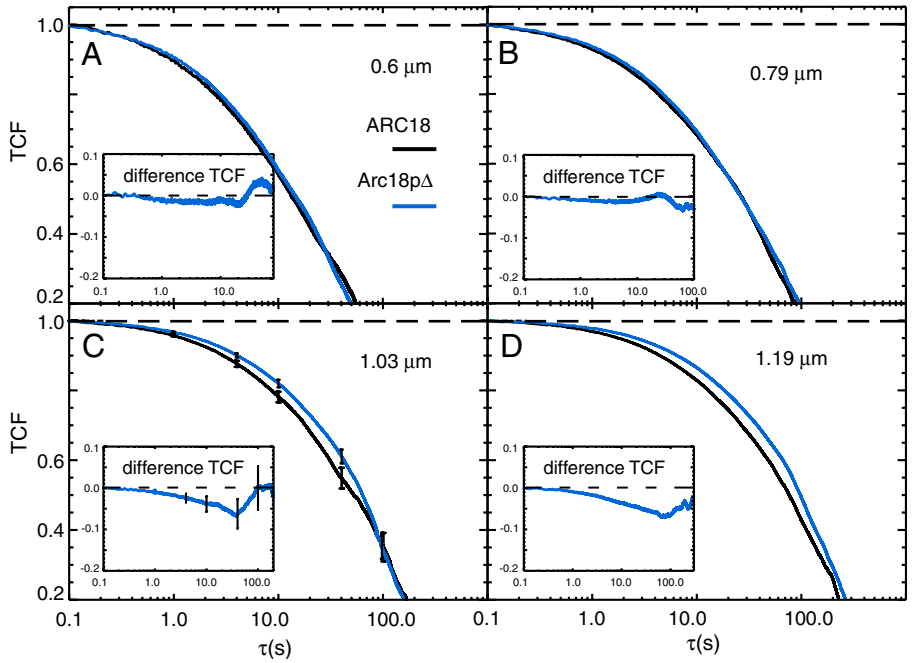

Fig. S5. Time correlation functions for Arc18pΔ studies. We compare TCFs for the mutant Arc18pΔ cells (blue curves) to those of the wild-type parent ARC18 (black curves). Each panel represents a different value for the probed length scale. For the smallest two length scales investigated ($d_G = 0.60$ and 0.79 μm), the mutant and wild-type parent strains are nearly identical. For the largest two length scales ($d_G = 1.03$ and 1.19 μm), the mutant Arc18pΔ is slower than the wild-type parent. Error bars are presented in (*C*).

Table S1. Strains used in this study

Strain	Genotype	Source
MYY290	MATa, his3Δ200, leu2-3, ura3-52	(Smith and Yaffe, 1991)
DDY1493	MATa, act1-V159N::HIS3, his3Δ200, tub2-101, ura3-52, leu2-3	(Belmont and Drubin, 1998)
DDY1495	MATa, ACT1::HIS3, his3Δ200, tub2-101, ura3-52, leu2-3	(Belmont and Drubin, 1998)
BY4741	MATa, his3Δ1, leu2Δ0, ura3Δ0, met15Δ0	(Open Biosystems)
YSC1021-555365	MATa, arc18Δ;;kanMX, his3Δ1, leu2Δ0, ura3Δ0, met15Δ0	(Open Biosystems)

Table S2. Effective short- and long-time diffusion coefficients of mitochondria in healthy cells and cells treated with Latrunculin-A

	Healthy		Latrunculin-A	
Fringe size, μm	$\tilde{D}^S(cm^2s^{-1})/10^{-12}$ (time: 0.7–1 s)	$\tilde{D}^L(cm^2s^{-1})/10^{-12}$ (time: 70 s)	$\tilde{D}^S(cm^2s^{-1})/10^{-12}$ (time: 0.7–1 s)	$\tilde{D}^L(cm^2s^{-1})/10^{-12}$ (time: 70 s)
0.60	7.75	2.49	5.36	1.72
0.78	8.18	2.64	6.13	1.78
1.03	9.41	3.01	7.34	1.90
1.19	8.35	2.97	6.25	1.97

Table S3. Effective short- and long-time diffusion coefficients of mitochondria in wild-type parent DDY-1495 cells and act1-V159N mutant DDY-1493.

	Wild type		act1-V159N	
Fringe size, μm	$\tilde{D}^S(cm^2s^{-1})/10^{-12}$ (time: 0.7–1 s)	$\tilde{D}^L(cm^2s^{-1})/10^{-12}$ (time: 70 s)	$\tilde{D}^S(cm^2s^{-1})/10^{-12}$ (time: 0.7–1 s)	$\tilde{D}^L(cm^2s^{-1})/10^{-12}$ (time: 70 s)
0.60	7.05	2.70	7.32	2.57
0.78	6.73	2.34	7.48	2.97
1.03	7.84	2.78	7.73	3.41
1.19	7.00	2.31	6.13	2.90

Table S4. Effective short- and long-time diffusion coefficients of mitochondria in wild-type parent Arc18p and Arc18pΔ cells.

	Wild type		Arc18pΔ	
Fringe size, μm	$\tilde{D}^S(cm^2s^{-1})/10^{-12}$ (time: 0.7–1 s)	$\tilde{D}^L(cm^2s^{-1})/10^{-12}$ (time: 70 s)	$\tilde{D}^S(cm^2s^{-1})/10^{-12}$ (time: 0.7–1 s)	$\tilde{D}^L(cm^2s^{-1})/10^{-12}$ (time: 70 s)
0.60	10.4	2.56	9.20	2.72
0.78	12.2	3.06	10.6	2.83
1.03	12.0	3.13	9.19	2.85
1.19	11.6	3.32	8.16	2.70